



Proper-orthogonal decomposition of spatio-temporal patterns in fluidized beds

P. G. Cizmas^a, A. Palacios^{b,*}, T. O'Brien^c, M. Syamlal^d

^aDepartment of Aerospace Engineering, Texas A&M University, College Station, TX 77843-3141, USA

^bNonlinear Dynamics Group, Department of Mathematics and Statistics, San Diego State University, San Diego, CA 92182-7720, USA

^cNational Energy Technology Laboratory, Department of Energy, Morgantown, WV 26507-0880, USA

^dFluent, Inc., Morgantown, WV 26507-0880, USA

Received 23 October 2002; received in revised form 13 May 2003; accepted 9 June 2003

Abstract

Numerical simulations of the hydrodynamics of a fluidized bed are carried out to investigate the complex interaction between the gas and the solid particles, and to explore the utility of a reduced-order model based on the proper orthogonal decomposition (POD). The behavior of a fluidized bed is modeled using a “two-fluid” theory, which involves conservation of mass, momentum, energy and species equations for the two interpenetrating continua. These equations are solved using a numerical algorithm that employs a conservative discretization scheme with mixed implicit and explicit formulations. We conducted simulations of gas–solid interaction in a narrow (two-dimensional) bed filled with sand particles which was uniformly fluidized at minimum fluidization but with additional air flow through a central nozzle. Aided by the proper orthogonal decomposition, spatial dominant features are identified and separated from the spatio-temporal dynamics of the simulations. The most dynamic region of the gas–solid interaction is confined to the central channel caused by the jet. The flow within this structure is successfully captured by a few POD eigenfunctions. Phase-space plots further indicate the existence of low-dimensional dynamics within the central channel. This conclusion supports the validity of a reduced-order model for fluidized beds, which can then be constructed by projecting the governing equations onto the POD modes, as it is commonly done in the Galerkin method.

© 2003 Elsevier Ltd. All rights reserved.

PACS: 05.45.–a; 05.70.Ln; 47.11.+j

Keywords: Fluidization; Multiphase flow; Model reduction; Nonlinear dynamics

1. Introduction

Over the past decades, scientists and engineers have conducted an enormous amount of research, both experimental and theoretical, to understand the fluidization phenomenon, in which solid particles acquire fluid-like properties as a result of being levitated by fluid flow. A realistic model of fluidized-bed reactors must capture the effects of hydrodynamics, heat transfer, and reaction kinetics. Most models of these reactors have been based on empirical correlations. More recently, computational models have also been developed. Such models are derived from the conservation laws for mass, momentum, energy and species. The resulting

governing equations consist of large and strongly coupled systems of partial differential equations (PDEs).

Due to the high dimensionality of the PDEs that govern the transport phenomena in fluidized beds, it is not feasible to use analytical methods to solve these equations. Numerical methods are used instead to simulate the fluidization phenomena. The advent of high-performance computers and the development of advanced algorithms have allowed significant improvements in the accuracy of numerical simulations. From these simulations, however, it is rather difficult to identify dominant spatial features of the underlying gas–solid dynamics and to relate these features to specific interaction terms in the models. Another drawback is the relative long time that is required to numerically solve the PDEs. This is a problem particularly for on-line model-based diagnostics and control. To address the above issues, we explore in this work the development of a reduced-order model

* Corresponding author. Tel.: +1-619-594-6808;
fax: +1-619-594-6746.

E-mail address: palacios@euler.sdsu.edu (A. Palacios).

using the technique of proper orthogonal decomposition (POD).

In this study, using the MFIX code (Syamlal, 1998; Syamlal, Rogers, & O'Brien, 1994), a two-fluid hydrodynamic model is used to simulate a two-dimensional bed filled with sand particles. This bed is uniformly aerated across the bottom at minimum fluidization. Additional air is injected through a central nozzle to produce a jet. POD is used to extract the dominant spatial features directly from the numerical simulations. For instance, we are particularly interested in determining whether low-dimensional attractors can capture the overall features of bed dynamics. Because of the central jet, the motion of the bed is most significant in a central channel. The gas-particle flow within this structure is successfully captured by a few POD eigenfunctions, approximately six modes. Reconstructions with more modes capture higher-dimensional features such as flow along the sides of the channel.

A reduced-order model can then be constructed through a Galerkin method, in which the PDE model is projected onto the set of POD eigenfunctions to yield a system of ordinary differential equations. To the best of our knowledge, this method has not been applied to large systems of PDEs such as the one employed in this work. The reduced-order model has the potential to help us further investigate, at near real-time speeds, how fluids and solids interact when they are in contact with each other and how to control the interaction. Understanding this interaction can significantly impact the use of fluidization in engineering applications that include: petroleum distillation, coal combustion, coating (metals/polymers), solidification, and cracking of hydrocarbons in chemical reactors.

A quantitative comparison between the results of numerical simulations and experimental data is also very important. Such comparisons can be challenging, however, because the chaotic nature of the fluidization phenomenon makes it difficult to quantitatively compare instantaneous values of transient simulations with experiments. Additionally, certain variables such as void fraction are not readily available in the experiments. Halow, Fasching, Nicoletti, and Spenik (1993), however, have developed a method for measuring voidage distributions in fluidized beds using capacitance imaging. The ability of POD to reduce experimental and numerical data can be exploited to extract information from both experiments and simulations that could be systematically compared for validation purposes. The purpose of the present work, however, is not to validate the results of numerical simulations based on the two-fluid model against experimental data, but to investigate the validity and merits of the POD based solely on snapshots generated by numerical simulations.

This paper is organized as follows. Section 2 presents a brief introduction to the fluidization phenomenon and a description of a two-fluid model that we employ to simulate gas–solid interactions. Section 3 presents basic ideas and properties of the proper orthogonal decomposition relevant

to this work. In particular, a theoretical description and a computational implementation for numerical simulations or experimental data are provided. Section 4 describes the results of applying the proper orthogonal decomposition to computer simulations of the two-fluid hydrodynamic model. The results support the existence of low-dimensional dynamics and suggest that building reduced-order models via Galerkin methods can be successful. This latter task is part of future work.

2. Fluidized beds

2.1. The fluidization phenomenon

Fluidization is the phenomenon in which a bed of solid particles acquire fluid-like properties (Fan & Zhu, 1997; Garg & Pritchett, 1975; Gidaspow, 1994; Gidaspow & Ettehadieh, 1983) due to the interstitial upward flow of a fluid through the bed. At low flow rates, the fluid percolates through the void spaces between the solids, which remains a packed bed; the forces acting on the bed due to the flow of the fluid is less than the weight of the bed. When the flow rate is increased above the minimum fluidization velocity, the solids become levitated due to the interaction between the fluid and the particles and the bed behaves like a fluid; it becomes fluidized. For most gas-particle systems, once this threshold is reached, voids that are shaped like bubbles, form and rise through the bed with vigorous motion and extensive coalescence and splitting (Boemer, Qi, & Renz, 1997; Cliff & Grace, 1985; Gera & Gautam, 1994, 1995; Zenz, 1968). If the fluid flow rate is further increased beyond the terminal velocity of the particles then the solids will be swept out of the container. For the particles studied in this work, Geldart Group B, bubbles are the major observable feature of the bed at the fluid velocities considered.

2.2. Governing equations

A complete description of the dynamics of solid particles suspended by the fluid can be achieved by coupling the Navier–Stokes equations for the fluid phase and the Newtonian equations for the solids (Patankar, Singh, Joseph, Glowinski, & Pan, 2000). This approach requires an enormous amount of computational time even with present computer technology. For practical purposes, a two-fluid hydrodynamic model is used to simulate gas–solid interactions (Anderson & Jackson, 1967; Gidaspow, 1994; Jackson, 1997). A computer code that solves the coupled PDEs of this model has been developed over the past 15 years at NETL (Syamlal et al., 1994). Based on fundamental laws of conservation of mass and momentum, the model describes the flow of dense or dilute fluid–solid mixtures. The model consists of the following system of partial

differential equations:

Conservation of mass

Gas mass balance:

$$\frac{\partial}{\partial t}(\varepsilon_g \rho_g) + \nabla \cdot (\varepsilon_g \rho_g \vec{v}_g) = 0. \quad (1)$$

Solids mass balance:

$$\frac{\partial}{\partial t}(\varepsilon_s \rho_s) + \nabla \cdot (\varepsilon_s \rho_s \vec{v}_s) = 0.$$

Conservation of momentum

Gas momentum balance:

$$\begin{aligned} \frac{\partial}{\partial t}(\varepsilon_g \rho_g \vec{v}_g) + \nabla \cdot (\varepsilon_g \rho_g \vec{v}_g \vec{v}_g) \\ = -\varepsilon_g \nabla P_g + \nabla \cdot \bar{\bar{\tau}}_g + F_{gs}(\vec{v}_s - \vec{v}_g) + \varepsilon_g \rho_g \vec{g}. \end{aligned}$$

Solids momentum balance:

$$\begin{aligned} \frac{\partial}{\partial t}(\varepsilon_s \rho_s \vec{v}_s) + \nabla \cdot (\varepsilon_s \rho_s \vec{v}_s \vec{v}_s) \\ = -\varepsilon_s \nabla P_g - \nabla \cdot \bar{\bar{S}}_s - F_{gs}(\vec{v}_s - \vec{v}_g) + \varepsilon_s \rho_s \vec{g}, \end{aligned} \quad (2)$$

where ε , ρ , and \vec{v} denote the volume fraction, density, and velocity; the subscripts g and s denote the gas phase and solids phase, respectively.

On the right in the gas momentum equation, the first term represent the normal surface forces, the second term the shear surface force. In the solids momentum equation, the first term on the right is due to the buoyant force of the fluid. The last two terms in both equations represent the drag force between the fluid and solids phases and gravitational body forces. No effects of stress in the granular phase were included in these calculations, except for the solids pressure.

2.3. Numerical simulations

The numerical algorithm used to solve hydrodynamic model equations (1) and (2) was developed at the Department of Energy's National Energy Technology Laboratory (Syamlal, 1998; Syamlal et al., 1994). The computer code, called MFIX (multiphase flow with interphase exchanges), is written in FORTRAN 90 and has the following capabilities: three-dimensional Cartesian and cylindrical coordinate systems, uniform or nonuniform grids, energy balances and gas and solids species balances. The output of the code includes time-dependent information on pressure, temperature, composition and velocity distribution in the reactors.

MFIX uses a staggered grid arrangement. The equations for scalar quantities (pressure, void fraction, temperature and mass fraction) are solved on the main grid. The equations for the velocity vector components are solved on staggered grids. Scalars are stored at cell centers and the components of velocity vector are stored at cell faces. The convective terms in mass and momentum equations can be differentiated using

first- or second-order accurate difference schemes. MFIX uses a mixed implicit and explicit formulation.

3. Proper orthogonal decomposition

The proper orthogonal decomposition is a well-known technique for determining an optimal basis for the reconstruction of a data set (Karhunen, 1946; Loeve, 1955). The POD has been used in various disciplines that include fluid mechanics (Berkooz, Holmes, & Lumley, 1993; Holmes, Lumley, & Berkooz, 1996; Lumley, 1967), identification and control in chemical engineering (Graham, Lane, & Luss, 1993), oceanography (Preisendorfer, 1988), image processing (Pratt, 1991) and flutter prediction (Pettit & Beran, 2000). Depending on the discipline, the POD is also known as Karhunen–Loève decomposition, principal components analysis, singular systems analysis and singular value decomposition. This section reviews the definitions and properties of the proper orthogonal decomposition relevant to this work and discusses how the method can be applied to computer simulations in order to separate spatial and temporal behavior.

3.1. Theoretical aspects

Let us consider a sequence of numerical and/or experimental observations represented by scalar functions $u(\mathbf{x}, t_i)$, $i = 1, \dots, M$. These functions are assumed to form a linear ($M \neq \infty$) infinite-dimensional Hilbert space L^2 (Riesz & Sz.-Nagy, 1990) on a domain D which is a bounded subset of \mathbb{R}^n , and they are parametrized by t_i which represents time. The time-average of the sequence, defined by

$$\bar{u}(\mathbf{x}) = \langle u(\mathbf{x}, t_i) \rangle = \frac{1}{M} \sum_{i=1}^M u(\mathbf{x}, t_i) \quad (3)$$

is assumed to be zero, without loss of generality. The proper orthogonal decomposition extracts time-independent orthonormal basis functions, $\Phi_k(\mathbf{x})$, and time-dependent orthonormal amplitude coefficients, $a_k(t_i)$, such that the reconstruction

$$u(\mathbf{x}, t_i) = \sum_{k=1}^M a_k(t_i) \Phi_k(\mathbf{x}), \quad i = 1, \dots, M \quad (4)$$

is optimal in the sense that the average least-squares truncation error

$$\epsilon_m = \left\langle \left\| u(\mathbf{x}, t_i) - \sum_{k=1}^m a_k(t_i) \Phi_k(\mathbf{x}) \right\|^2 \right\rangle \quad (5)$$

is a minimum for any given number $m \leq M$ of basis functions over all possible sets of orthogonal functions. Here $\|\cdot\|$ is the L^2 -norm $\|f\|^2 = (f, f)$, where (\cdot, \cdot) denotes the standard Euclidean inner product. The functions $\Phi_k(\mathbf{x})$

are called *empirical eigenfunctions*, *coherent structures*, or *POD modes*.

Optimality property (5) is equivalent to finding functions Φ that maximize the normalized average projection of u onto Φ

$$\max_{\Phi \in L^2(D)} \frac{\langle |u, \Phi|^2 \rangle}{\|\Phi\|^2}, \quad (6)$$

where $|\cdot|$ denotes the modulus. Optimum condition (6) reduces to the eigenvalue problem (Berkooz et al., 1993)

$$\int_D \langle u(\mathbf{x})u^*(\mathbf{y}) \rangle \Phi(\mathbf{y}) \, d\mathbf{y} = \lambda \Phi(\mathbf{x}), \quad (7)$$

where $\mathbf{x}, \mathbf{y} \in D$. Consequently, the optimal basis functions $\{\Phi_k\}$ are the eigenfunctions of integral equation (7), whose kernel is the averaged *autocorrelation* function

$$\langle u(\mathbf{x})u^*(\mathbf{y}) \rangle \equiv R(\mathbf{x}, \mathbf{y}).$$

In practice, the state of a numerical model is only available at discrete spatial grid points, so that the observations that form the data set are vectors rather than continuous functions. In other words, $D = (x_1, x_2, \dots, x_N)$, where x_j is the j th grid point and $u(\mathbf{x}, t_i)$ is the vector $\mathbf{u}_i = [u(x_1, t_i), u(x_2, t_i), \dots, u(x_N, t_i)]^T$. The data set can be obtained from numerical simulation, experimental investigation or a combination of the numerical and experimental results. In the discrete case, the autocorrelation function is replaced by the tensor product matrix

$$R(\mathbf{x}, \mathbf{y}) = \frac{1}{M} \sum_{i=1}^M \mathbf{u}_i \mathbf{u}_i^T. \quad (8)$$

More importantly, it can also be shown that the eigenvectors of the $R(\mathbf{x}, \mathbf{y})$ matrix yield the eigenfunctions $\Phi_k(\mathbf{x})$, which can be computed with the algorithm presented in Section 3.2.

3.2. Computational implementation: method of snapshots

A popular technique for finding the eigenvectors of Eq. (8) is the *method of snapshots* developed by Sirovich (1987). It was introduced as an efficient method when the resolution of the spatial domain (N) is higher than the number of observations (M). The method of snapshots is based on the fact that the data vectors, \mathbf{u}_i , and the eigenvectors Φ_k , span the same linear space (Holmes et al., 1996; Sirovich, 1987). This implies that the eigenvectors can be written as a linear combination of the data vectors

$$\Phi_k = \sum_{i=1}^M v_i^k \mathbf{u}_i, \quad k = 1, \dots, M. \quad (9)$$

After substitution in the eigenvalue problem, $R(\mathbf{x}, \mathbf{y})\Phi(\mathbf{y}) = \lambda \Phi(\mathbf{x})$, the coefficients v_i^k are obtained from the solution of

$$C\mathbf{v} = \lambda \mathbf{v}, \quad (10)$$

where $\mathbf{v}^k = (v_1^k, \dots, v_M^k)$ is the k th eigenvector of Eq. (10), and C is a symmetric $M \times M$ matrix defined by $[C_{ij}] = (1/M)(\mathbf{u}_i, \mathbf{u}_j)$. Here (\cdot, \cdot) denotes the standard vector inner product, $(\mathbf{u}_i, \mathbf{u}_j) = u(x_1, t_i)u(x_1, t_j) + \dots + u(x_N, t_i)u(x_N, t_j)$. In this way the eigenvectors of the $N \times N$ matrix R (8) can be found by computing the eigenvectors of an $M \times M$ matrix C (10), a preferable task if $N \gg M$. The results presented in Section 4 were obtained with an implementation of the method of snapshots. An iterative QR method (Stewart & Leyk, 1994) was used to compute the eigenvectors of the symmetric matrix C from Eq. (10).

Once the POD modes are computed, the Galerkin procedure can be applied to reduce a set of PDEs to a smaller set of ODEs. Given a PDE model of the form $\partial u / \partial t = F(u)$, the Galerkin procedure consists of using the POD decomposition of u shown in Eq. (4) to generate a reduced set of ODEs by solving the equations

$$\left(\Phi_j, \sum_{k=1}^M \frac{da_k}{dt} \Phi_k(\mathbf{x}) - F \left(\sum_{k=1}^M a_k(t_i) \Phi_k(\mathbf{x}) \right) \right) = 0, \\ j = 1, \dots, M.$$

Note that the dependent variables of the set of ODEs are the POD amplitude coefficients. For further details, the reader is referred to Fletcher (1984).

3.3. Properties of the proper orthogonal decomposition

Since the kernel is Hermitian, $R(\mathbf{x}, \mathbf{y}) = R^*(\mathbf{y}, \mathbf{x})$, according to the Riesz Theorem (Riesz & Sz.-Nagy, 1990), it admits a diagonal decomposition of the form

$$R(\mathbf{x}, \mathbf{y}) = \sum_{k=1}^M \lambda_k \Phi_k(\mathbf{x}) \Phi_k^*(\mathbf{y}). \quad (11)$$

This fact is particularly useful when finding the POD modes analytically. They can be read from diagonal decomposition (11). The temporal coefficients, $a_k(t_i)$, are calculated by projecting the data set on each of the eigenfunctions

$$a_k(t_i) = (u(\mathbf{x}, t_i), \Phi_k(\mathbf{x})), \quad i = 1, \dots, M. \quad (12)$$

It can be shown that both temporal coefficients and eigenfunctions are uncorrelated in time and space, respectively (Holmes et al., 1996; Sirovich, 1987). That is, the following orthogonality properties hold:

- (i) $\Phi_j^*(\mathbf{x})\Phi_k(\mathbf{x}) = \delta_{jk}$,
- (ii) $\langle a_j(t_i)a_k^*(t_i) \rangle = \delta_{jk}\lambda_j$,

where δ_{jk} represents the Kronecker delta function.

Property (ii) is obtained when the terms in diagonal decomposition (11) are compared with the expression $R(\mathbf{x}, \mathbf{y}) = \sum \langle a_j(t_i)a_k^*(t_i) \rangle \Phi_j(\mathbf{x})\Phi_k^*(\mathbf{y})$. The nonnegative and self-adjoint properties of $R(\mathbf{x}, \mathbf{y})$ imply that all eigenvalues are nonnegative and can be ordered accordingly:

$\lambda_1 \geq \lambda_2 \geq \dots \geq \lambda_k \geq \dots \geq 0$. Statistically speaking, λ_k represents the variance of the data set in the direction of the corresponding POD mode, $\Phi_k(\mathbf{x})$. In physical terms, if u represents a component of a velocity field, then λ_k measures the amount of kinetic energy captured by the respective POD mode, $\Phi_k(\mathbf{x})$. In this sense, the energy measures the contribution of each mode to the overall dynamics.

The total energy captured in a proper orthogonal decomposition of a numerical or experimental data set is defined as the sum of all eigenvalues

$$E = \sum_{k=1}^m \lambda_k. \tag{13}$$

The relative energy captured by the k th mode, E_k , is defined by

$$E_k = \frac{\lambda_k}{\sum_{j=1}^m \lambda_j}. \tag{14}$$

Note that the cumulative sum of relative energies, $\sum E_k$, approaches one as the number of modes in the reconstruction increases.

Table 1
System parameters

Parameter	Value
Particles dimension	500 μm
Particles density	2610 kg/m^3
Gas temperature	297 K
Gas pressure	101 kPa
Bed size	0.39 m width \times 0.58 m height
Grid size	128 \times 108

4. Results

The MFIX code was used to simulate the fluidization phenomenon in a two-dimensional bed filled with sand particles. This fluidization process has been experimentally investigated by Gidaspow (1994). The bed was fluidized uniformly at minimum fluidization, with additional gas injected through a central jet. The parameters used in the numerical simulation are presented in Table 1.

The central jet produces a spatio-temporal flow pattern that is easier to analyze than that with uniform excess gas flow through the distributor. Fig. 1 depicts the

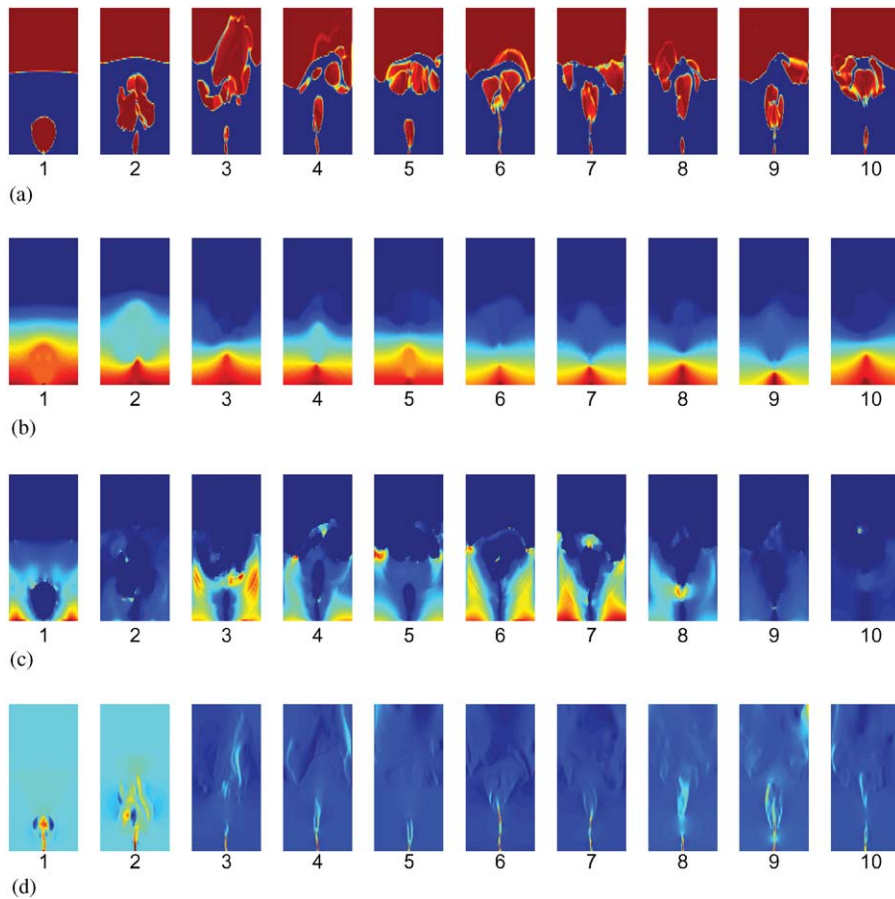


Fig. 1. Simulation of fluidization with a central jet. Gas is injected into a two-dimensional fluidized bed filled with sand particles. Time evolves from left to right: (a) ϵ_g : volume fraction of fluid phase, (b) P_g : gas pressure, (c) P_s : solids pressure, (d) v_g : gas velocity along the y -axis.

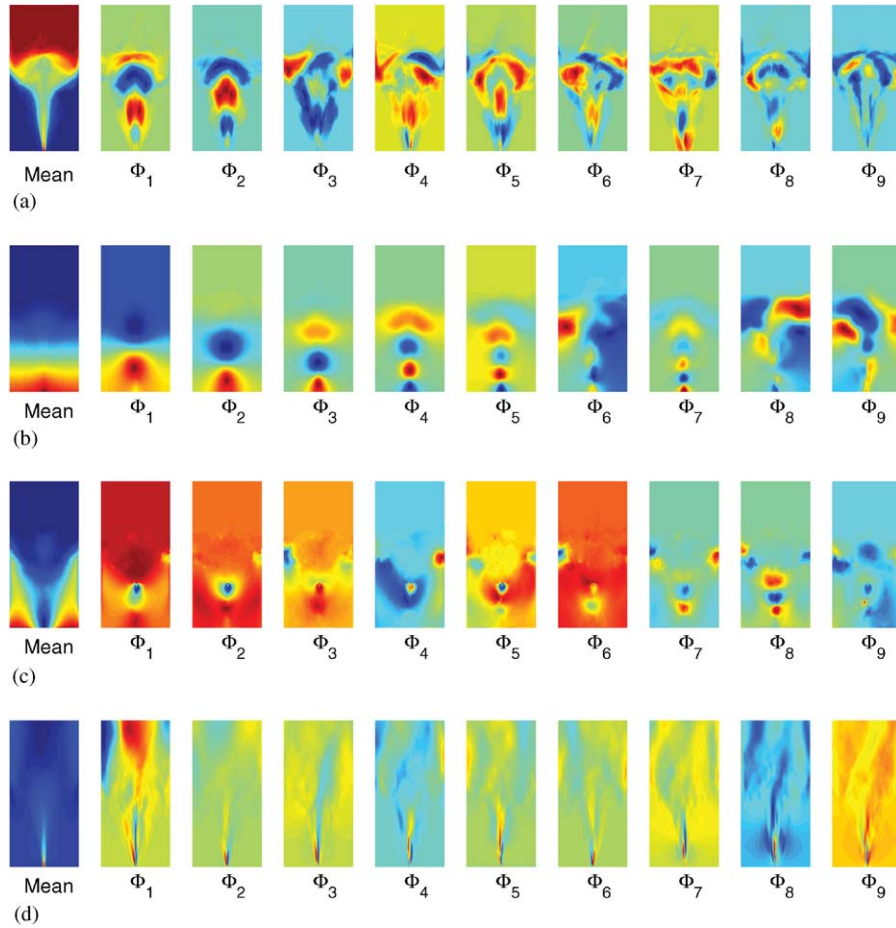


Fig. 2. Mean and POD spatial features extracted from simulations of Fig. 1: (a) ε_g : volume fraction of fluid phase, (b) P_g : gas pressure, (c) P_s : solids pressure, (d) v_g : gas velocity along the y -axis.

spatio-temporal evolution of several of the dependent variables of the model. ε_g is the voidage, the local volume fraction of the fluid phase, which describes the fraction of the bed occupied by the interstitial gas; P_g is the gas pressure; P_s is the solids phase pressure, and v_g is the component of the gas velocity in the vertical direction. No scales are shown for these variables. The figure is intended to present the time evolution of these variables.

Fig. 2 shows the 10 most energetic spatial modes (including the mean) obtained after applying the proper orthogonal decomposition to simulations shown in Fig. 1. Observe that the time-average of each variable, which can be considered mode Φ_0 , has an approximate reflective symmetry, which mimics the symmetry of the experiment. More remarkable is the fact that the reflective symmetry appears even though none of the time instantaneous snapshots have this symmetry, as is shown in Fig. 1(a). Shading in this and other similar figures is done such that high-quantity values are colored red, low-quantity values are colored blue, and intermediate values are colored through a linear interpolation between red and blue.

Recall that the motivation for applying the proper orthogonal decomposition is to obtain information about the long-term behavior of the fluidized-bed system. Suppose that this behavior is captured by an attractor, denoted by \mathcal{A} (see Hale (1980) for a precise definition). Assume that $\mathbf{g}(\mathbf{x}, t_i)$, $i = 1, \dots, M$, represents the scalar spatio-temporal measurements produced by numerical simulations or experimental work. In practice, one must first compute the time-average

$$\bar{\mathbf{g}}(\mathbf{x}) = \frac{1}{M} \sum_{i=1}^M g(\mathbf{x}, t_i),$$

in order to produce a new set of measurements, $u(\mathbf{x}, t_i) = g(\mathbf{x}, t_i) - \bar{g}(\mathbf{x})$, with zero average. Let Γ denote the symmetry group of the system of interest. The symmetries of the attractor form a subgroup of Γ defined by

$$\Gamma_{(\mathcal{A})} = \{\gamma \in \Gamma \mid \gamma\mathcal{A} = \mathcal{A}\}. \quad (15)$$

Dellnitz, Golubitsky, and Nicol (1994) made the critical observation that symmetries of attractors of partial

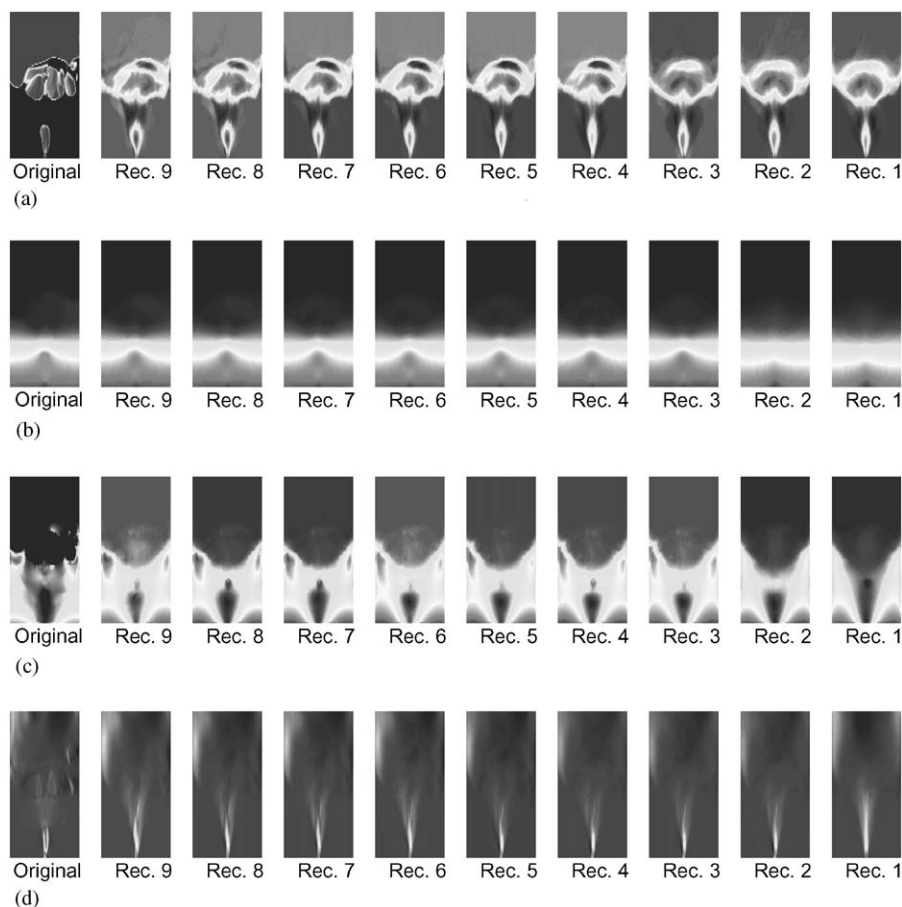


Fig. 3. Sequence of reconstructions (rec.) with successively higher-order POD modes for the simulations shown in Fig. 1. Time is held fixed at $t = 100$. Level of detail increases from right to left, with the highest-order reconstruction next to the original image. (a) ε_g : Volume fraction of fluid phase, (b) P_g : gas pressure, (c) P_s : solids pressure, (d) v_g : gas velocity along the y -axis.

differential equations, such as two-fluid model equations (1) and (2), appear as symmetries of the time-average, $\bar{g}(\mathbf{x})$, independently of the symmetries of the instantaneous scalar field $g(\mathbf{x}, t_i)$. Unfortunately, the converse is not always true. The symmetries of the time-average do not necessarily reflect the symmetries of the underlying attractor. This implies that reduced-order models obtained via Galerkin projections from partial differential equations onto POD modes might lead to ordinary differential equations with more symmetry than is present in an actual numerical simulation or experimental investigation (Dellnitz et al., 1994). There are, however, various methods which ensure that the reduced Galerkin models can retain the same symmetry properties of the original system. For instance, Sirovich (1987) has proposed that data sets be enlarged by symmetry operations prior to performing the POD decomposition. Dellnitz et al. (1994) have also proposed a method for constructing an appropriate reduced-order model by combining the POD decomposition with the computation of the symmetry type of the underlying attractor using *detectives*. An additional procedure, called “template fitting”, has also been proposed more recently (Rowley & Marsden, 2000).

These procedures will be taken into consideration in future work.

As shown in Fig. 2, the time-average and the POD modes of all representative variables have a channel structure where the main flow motion is confined. Computer animations of the reconstructed flow with increasing numbers of POD modes, from one to 10 (including the time-average), were performed and compared with the original simulations. Visual inspection of these animations reproduce the overall motion through the middle of the channel structure. For example, Fig. 3 shows a time snapshot of various reconstructions with successively higher-order POD modes of the variables shown in Fig. 1. Each reconstructed snapshot (rec. 1–9) was computed using a partial sum $m < M$ of Eq. (4), with time held fixed at $t = 100$. As the number of modes increases, each individual reconstructed image shows less reflectional symmetry. In addition, high-dimensional features, such as motion along the sides of the channel, become more visible. In the particular case of gas pressure, P_g , the time-average and the first four POD modes reveal a layer structure with different pressure values that run from the bottom to the middle of the bed. A careful examination of POD

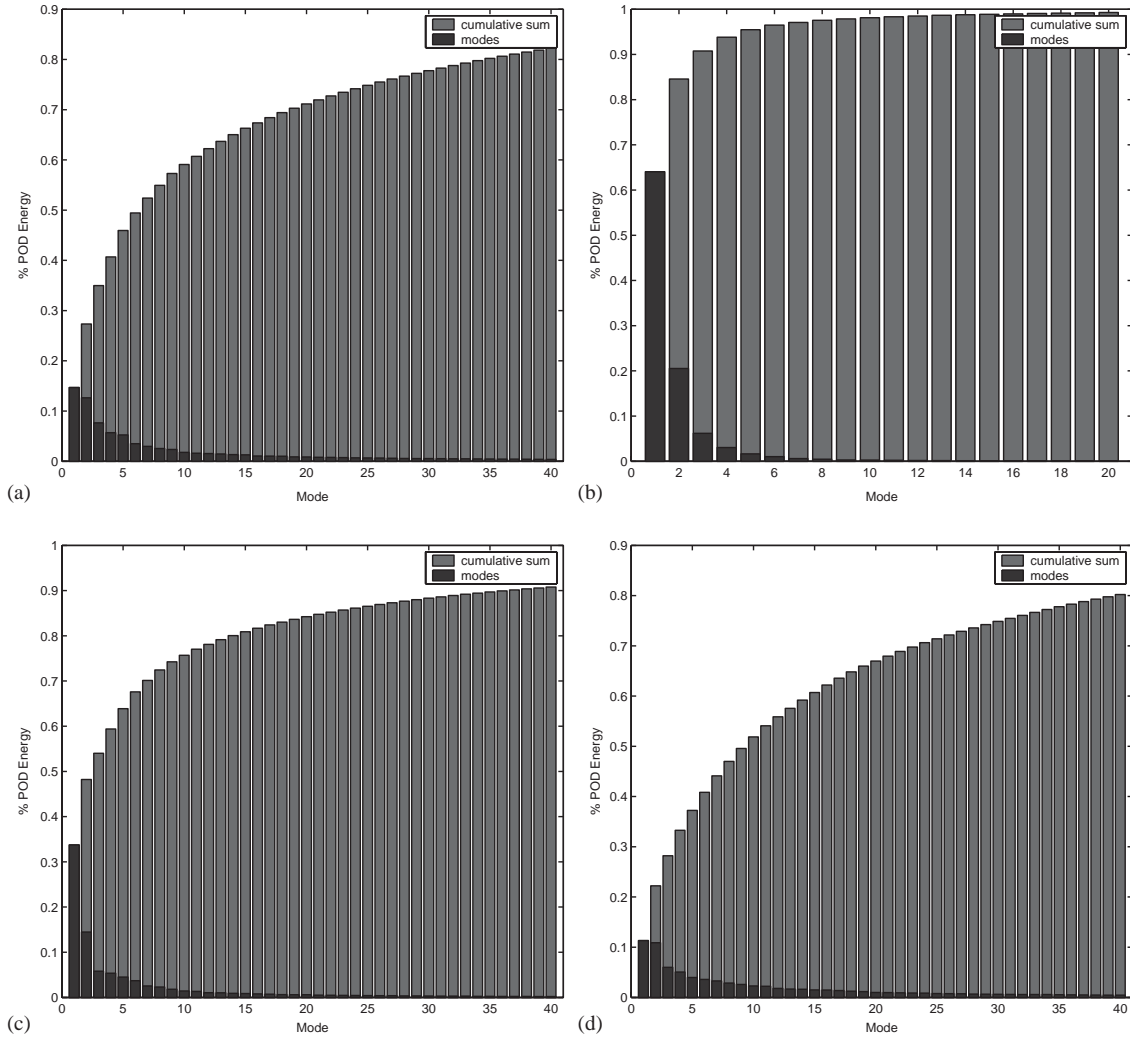


Fig. 4. POD energy spectrum of some representative spatio-temporal variables: (a) ε_g , (b) P_g , (c) P_s , (d) v_g .

reconstructions indicates, however, that the circular features that appear in some of the modes are physically related to the burst of gas pressure that emanates from the nozzle located at the bottom-center of the bed. Both the channel structure of the flow and the layer structure of gas pressure are consistent with reported experimental work (Kuipers, Tammes, Prins, & van Swaaij, 1992).

The POD energy spectrum of the sampled variables is shown in Fig. 4. The spectrum of gas pressure shows that more than 85% of the POD energy is captured by the first two modes, which form a layer structure. We can also observe that the POD energy increases rapidly as the number of modes increases. Such rapid roll-off of energy can be attributed to the fact that spatial variations in gas pressure are relatively close to its time-average; the gas pressure is inherently spatially averaged. This conclusion strongly suggests that the spatio-temporal dynamics of gas pressure is low dimensional, which is encouraging with respect to building a reduced-order model. The spectra of the other variables show that more modes are necessary in order to

Table 2

POD energy vs number of modes for ε_g , P_g , P_s and V_g

POD energy (%)	Number of modes			
	ε_g	P_g	P_s	V_g
80	34	2	14	40
85	43	3	20	68
90	77	4	34	123
95	214	5	70	356
99	480	20	395	490

capture high-dimensional features of their dynamics, such as details of the flow near the walls. The number of modes necessary to capture various levels of the POD energy are shown in Table 2. The exact number of modes employed in Galerkin reductions is typically chosen based on empirical considerations. Some authors (Sirovich, 1987) recommend a nominal criterion of using as many modes as necessary to capture 99% of the energy, though there are cases where

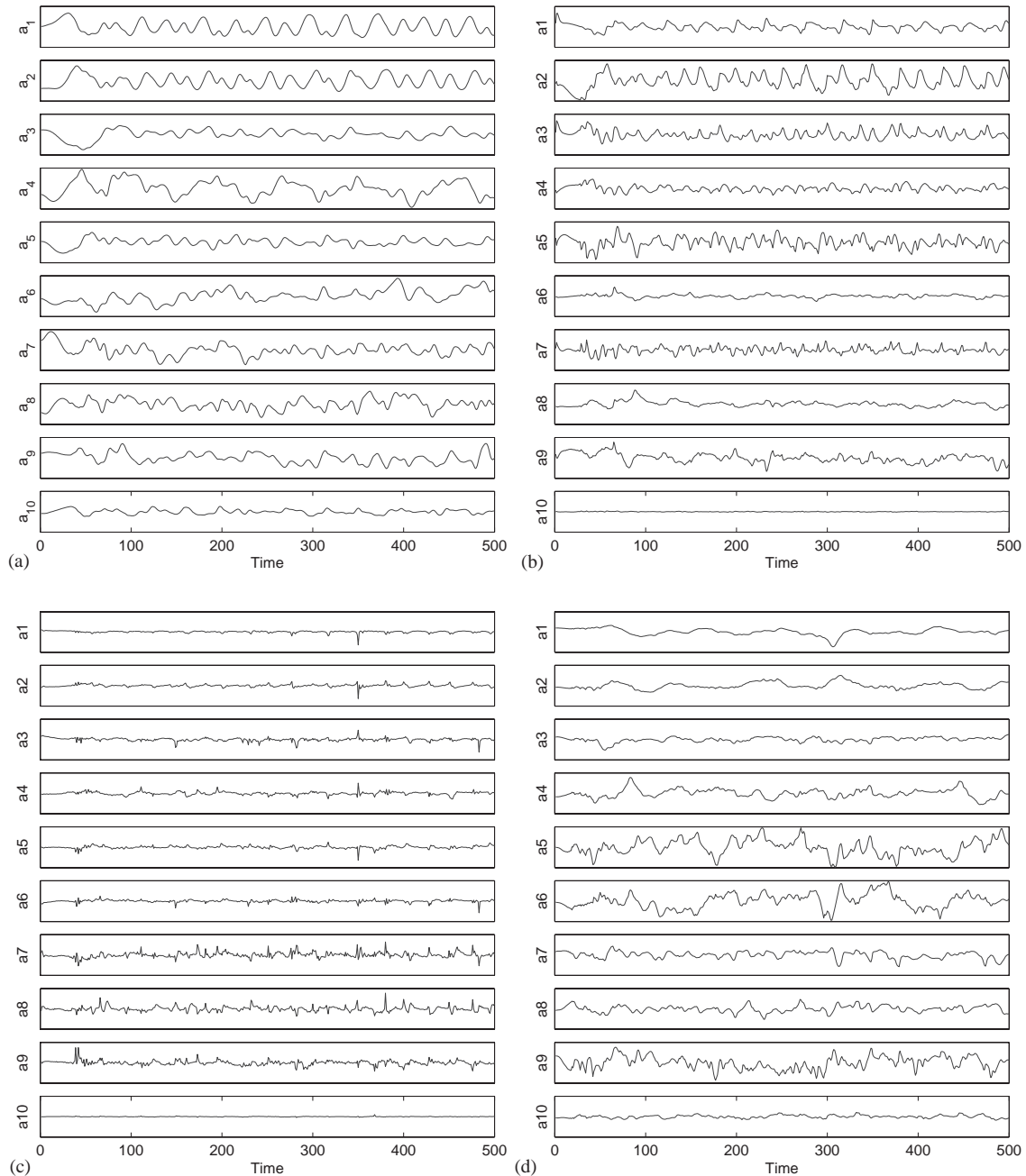


Fig. 5. Time evolution of POD amplitude coefficients in the 10-mode decomposition of the gas jet simulation: (a) ε_g , (b) P_g , (c) P_s , (d) v_g .

a 75% cut-off suffices to capture low-dimensional effects only (Palacios, Gunaratne, Gorman, & Robbins, 1998). In our case, finding an energy cut-off depends greatly on how important the high-dimensional wall effects are. On the other hand, if the priority is to construct a model that can capture the overall dynamics within the central channel, then fewer modes might be adequate. This issue will be further investigated in future work.

In order to choose a set of orthogonal POD modes for the Galerkin reduction or projection, we should consider first that the simulations of Fig. 1 were obtained by integrating

two-fluid models (1) and (2) over a rectangular domain of 124×108 grid points, which can be considered as $\mathbf{R}^{124 \times 108}$. Since the POD modes obtained from these simulations are orthonormal bases of $\mathbf{R}^{124 \times 108}$, then in principle, we could use the modes from any particular variable to represent the other variables. However, this was not attempted in this numerical study.

Fig. 5 shows the time-dependent amplitude coefficients associated with the reconstruction using the 10 POD modes of Fig. 2. These time series reveal some well-defined structures, which also support the existence of low-dimensional

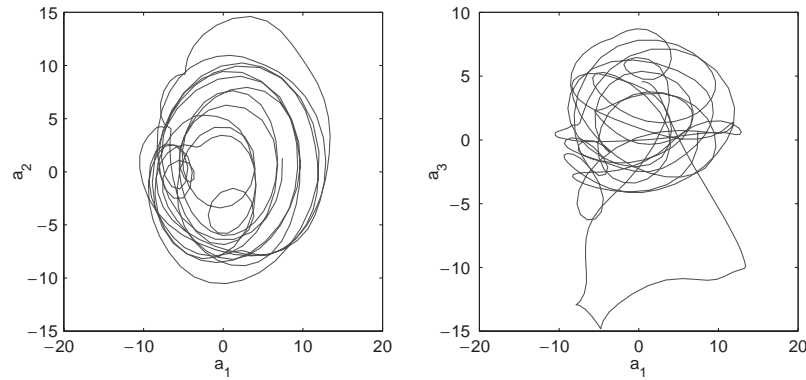


Fig. 6. Phase space projections of amplitudes coefficients obtained through the proper orthogonal decomposition of void fraction of the gas phase. The projection reveals low-dimensional dynamics in the form of cycling behavior.

deterministic dynamics. To gain insight into the actual structure of the attractor, we can use the time series to plot phase-space projections. For instance, Fig. 6 shows two projections from the amplitude coefficients associated with gas volume fraction, ε_g . The relatively closed nature of the resulting curves further illustrates the presence of a low-dimensional attractor. An animation of ε_g reconstructed with the three most energetic modes captures the overall variations of gas void fraction along the central channel which results in the time-average of Fig. 2(a).

5. Conclusions

Numerical simulations and POD of gas–solid interactions in a two-dimensional fluidized bed were carried out to explore the feasibility of deriving a reduced order model via Galerkin methods. The governing equations were written in strong conservation form and solved using the MFIX code. The focus of the work was on simulations of a bed of sand particles at uniform minimum fluidization, but with excess gas injected through a central jet. The proper orthogonal decomposition was used to identify and extract spatial dominant features from relevant spatio-temporal variables. The results indicate that a low number of POD modes can capture the overall characteristics of the motion, which on average, appears to be confined to a central channel formed from the bottom to the top of the bed. This channel structure contains, approximately, the reflective symmetry of the bed. Large number of modes are needed, however, if we are also interested in capturing the fine details of the spatial features of the flow near the central channel. Phase-space plots further illustrate the existence of a low-dimensional attractor with approximate reflective symmetry. Consequently, projecting the governing PDE model onto the POD modes, as is common practice for Galerkin methods, can lead to the desired reduced order models. The development of this last task is part of future work.

Notation

E	total energy per unit volume
F_{gs}	drag force between fluid and solids
\vec{g}	acceleration due to gravity
P	pressure
t	time in Cartesian coordinates
\vec{v}	velocity vector
(x, y)	Cartesian coordinates

Greek letters

ε	void fraction
μ	viscosity
ρ	density
$\bar{\tau}_g$	deviatoric stress tensor
Φ	basis function

Superscripts

–	time average
*	complex conjugate

Subscripts

g	gas phase
POD	POD reconstruction solution
s	solids phase

Acknowledgements

This work has been funded by the Department of Energy through Grant DE-FC26-00NT40903. We would like to thank Dr. C. Guenther and Mr. J. Rockey of the National Energy Technology Laboratory, Dr. S. Daw of the Oak Ridge National Laboratory, Prof. M. Golubitsky of the University of Houston, and Prof. K. Robbins of the University of Texas at San Antonio for many fruitful discussions and suggestions.

References

- Anderson, T. B., & Jackson, R. (1967). A fluid mechanical description of fluidized beds. *Industrial and Engineering Chemistry, Fundamentals*, 6, 527–539.
- Berkooz, G., Holmes, P., & Lumley, J. L. (1993). The proper orthogonal decomposition in the analysis of turbulent flows. *Annual Review of Fluid Mechanics*, 25, 539–575.
- Boemer, A., Qi, H., & Renz, U. (1997). Eulerian simulation of bubble formation at a jet in a two-dimensional fluidized bed. *International Journal of Multiphase Flow*, 5, 927–944.
- Clift, R., & Grace, J. R. (1985). Bubble interaction in fluidized beds. *International Journal of Multiphase Flow*, 105, 14–27.
- Dellnitz, M., Golubitsky, M., & Nicol, M. (1994). Symmetry of attractors and the Karhunen–Loève decomposition. In L. Sirovich (Ed.), *Trends and perspectives in applied mathematics* (pp. 73–108). New York: Springer.
- Fan, L., & Zhu, C. (1997). *Principles of gas–solid flows*. New York: Cambridge University Press.
- Fletcher, C. A. J. (1984). *Computational Galerkin methods*. Berlin: Springer.
- Garg, S. K., & Pritchett, J. W. (1975). Dynamics of gas-fluidized beds. *Journal of Applied Physics*, 46, 4493–4500.
- Gera, D., & Gautam, M. (1994). Variation of throughflow velocity in a 2-d rising bubble. *Powder Technology*, 79, 257–263.
- Gera, D., & Gautam, M. (1995). Bubble rise velocity in two-dimensional fluidized beds. *Powder Technology*, 84, 283–285.
- Gidaspow, D. (1994). *Multiphase flow and fluidization*. Boston: Academic Press.
- Gidaspow, D., & Etehadieh, B. (1983). Fluidization in two-dimensional beds with a jet; part 2: Hydrodynamic modeling. *Industrial and Engineering Chemistry, Fundamentals*, 22, 193–201.
- Graham, M. D., Lane, S. L., & Luss, D. (1993). Proper orthogonal decomposition analysis of spatiotemporal temperature patterns. *Journal of Physical Chemistry*, 97(4), 889–894.
- Hale, J. K. (1980). *Ordinary differential equations*. New York: Wiley.
- Halow, J. S., Fasching, G. E., Nicoletti, P., & Spenik, J. L. (1993). Observations of a fluidized bed using capacitance imaging. *Chemical Engineering Science*, 48(4), 643–659.
- Holmes, P., Lumley, J. L., & Berkooz, G. (1996). *Turbulence, coherent structures, dynamical systems and symmetry*. Cambridge: Cambridge University Press.
- Jackson, R. (1997). Locally averaged equations of motion for a mixture of identical spherical particles and a newtonian fluid. *Chemical Engineering Science*, 52, 2457–2469.
- Karhunen, K. (1946). Zur spektraltheorie stochastischer. *Annales Academiae Scientiarum Fennicae Series A*, 1, 34.
- Kuipers, J. A. M., Tammes, H., Prins, W., & van Swaaij, W. P. M. (1992). Experimental and theoretical porosity profiles in a two-dimensional gas-fluidized bed with a central jet. *Powder Technology*, 71, 87–99.
- Loeve, M. (1955). *Probability theory*. New York: Van Nostrand.
- Lumley, J. L. (1967). The structure of inhomogeneous turbulent flows. In A. M. Yaglom, & V. I. Tatarski (Eds.), *Atmospheric turbulence and radio wave propagation* (pp. 167–178). Moscow: Nauka.
- Palacios, A., Gunaratne, G., Gorman, M., & Robbins, K. (1998). A Karhunen–Loève analysis of spatiotemporal flame patterns. *Physical Review E*, 57(5), 5958–5971.
- Patankar, N. A., Singh, P., Joseph, D. D., Glowinski, R., & Pan, T.-W. (2000). A new formulation of the distributed lagrange multiplier/fictitious domain method for particulate flows. *International Journal of Multiphase Flow*, 26, 1509–1524.
- Pettit, C. L., & Beran, P. S. (2000). Reduced-order modeling for flutter prediction. In *41st AIAA/ASCE/AHS/ASC structural, structural dynamics and materials conference*, Atlanta, GA.
- Pratt, K. W. (1991). *Digital image processing* (2nd ed.). New York: Wiley.
- Preisendorfer, R. (1988). In C. Mobley (Ed.), *Principal component analysis in meteorology and oceanography*. Amsterdam: Elsevier.
- Riesz, F., & Sz.-Nagy, B. (1990). *Functional analysis*. New York: Dover.
- Rowley, C. W., & Marsden, J. (2000). Reconstruction equations and the Karhunen–Loève expansion for systems with symmetry. *Physica D*, 142, 1–19.
- Sirovich, L. (1987). Turbulence and the dynamics of coherent structures. *Quarterly of Applied Mathematics*, 5, 561–590.
- Stewart, D. E., & Leyk, Z. (1994). Meschach: Matrix computations in c. In *CMA proceedings no. 32*, Australian National University, Canberra, Australia.
- Syamlal, M. (1998). *MFIX documentation: Numerical technique*. Technical report DOE/MC-31346-5824. NTIS/DE98002029, DOE/MC.
- Syamlal, M., Rogers, W., & O'Brien, T. J. (1994). *MFIX documentation theory guide*. Technical report DOE/METC-94/1004, DOE/METC.
- Zenz, F. A. (1968). Bubble formation and grid design. *Institution of Chemical Engineering Symposium Series*, 30, 136–139.